Geophysical Journal International

Geophys. J. Int. (2024) **236,** 290–304
Advance Access publication 2023 October 20
GJI Heat Flow and Volcanology

https://doi.org/10.1093/gji/ggad415

Numerical thermomechanical modelling of lava dome growth during the 2007–2009 dome-building eruption at Volcán de Colima

Natalya Zeinalova,[1] Alik Ismail-Zadeh,[1] Igor Tsepelev,[2] Oleg Melnik[3] and Frank Schilling[1]

[1]*Karlsruhe Institute of Technology, Department of Civil Engineering, Geo and Environmental Sciences, Institute of Applied Geosciences, 76131 Karlsruhe, Germany. E-mail: alik.ismail-zadeh@kit.edu*
[2]*Institute of Mathematics and Mechanics, Ural Branch of the Russian Academy of Sciences, 620108 Yekaterinburg, Russia*
[3]*ISTerre, University Grenoble Alpes, 38058 Grenoble, France*

Accepted 2023 October 18. Received 2023 October 16; in original form 2022 November 19

SUMMARY

Lava domes form during effusive eruptions due to an extrusion of highly viscous magmas from volcanic vents. In this paper we present a numerical study of the lava dome growth at Volcán de Colima, Mexico during 2007–2009. The mathematical model treats the lava dome extrusion dynamics as a thermomechanical problem. The equations of motion, continuity and heat transfer are solved with the relevant boundary and initial conditions in the assumption that magma viscosity depends on the volume fraction of crystals and temperature. We perform several sets of numerical experiments to analyse the internal structure of the lava dome (i.e. the distributions of the temperature, crystal content, viscosity and velocity) depending on various heat sources and thermal boundary conditions. Although the lava dome growth at Volcán de Colima during short (a few months) dome-building episodes can be explained by an isothermal model of lava extrusion with the viscosity depending on the volume fraction of crystals, we show here that cooling plays a significant role during long (up to several years) episodes of dome building. A carapace develops as a response to a convective cooling at the lava dome–air interface. The carapace becomes thicker if the radiative heat loss at the interface is also considered. The thick carapace influences the lava dome dynamics preventing its lateral advancement. The release of the latent heat of crystallization leads to an increase of the temperatures in the lava dome interior and to a relative flattening of the dome. Meanwhile, the heat source due to viscous dissipation inside the lava dome is negligible, and it does not influence the lava dome growth. The developed thermomechanical model of the lava dome dynamics at Volcán de Colima can be used elsewhere to analyse effusive eruptions, dome morphology and carapace evolution including its failure potentially leading to pyroclastic flow hazards.

Key words: Numerical modelling; Lava rheology and morphology; Heat transfer; Crystallization; Volcán de Colima.

1 INTRODUCTION

An effusive eruption of highly viscous magma leads to a lava dome growth in the volcanic crater interrupted by its collapse due to gas pressure building-up or gravitational instability. The collapse events may completely or in part remove the dome and result in pyroclastic density currents—high-speed avalanches of rocks and ashes. The thermomechanical structure of a lava dome interior (i.e. the temperature, the crystal content and the lava viscosity) is poorly known. However, this knowledge is critical for assessment of potential dome collapse and related hazards (e.g. Voight & Elsworth 2000; Watts *et al.* 2002).

Lava dome dynamics is governed by crystallization and outgassing of the viscous magma in the volcanic conduit (Melnik & Sparks 1999). The domes represent extrusions of a high viscous magma from a volcanic vent, which are affected by degassing, crystallization and cooling. Lava dome morphology varies with the discharge rate, the kinetics of the crystal content growth, the temperature and the vent geometry (e.g. Tsepelev *et al.* 2020; Mériaux *et al.* 2022). A highly viscous dome-forming magma prevents significant lateral advancement of the extruded lava from the vent compared to a less viscous lava, which flows along the volcano's topographic slope. At low eruption rates, lava dome dynamics is associated with high groundmass crystallinity and

substantial yield strength (e.g. Lavallée *et al.* 2012; Calder *et al.* 2015; Sheldrake *et al.* 2016). Due to cooling, domes develop a 'solid' carapace (a highly viscous surface layer of the dome). This carapace remains deformable for days to months (Anderson & Fink 1990) influencing the dome morphology (Iverson 1990) because of the mobility of less viscous lava within the interior of the dome.

Lava dome growth has been monitored at several volcanoes (e.g. Nakada *et al.* 1999, 2019; Watts *et al.* 2002; Harris *et al.* 2003; Wadge *et al.* 2014; Zobin *et al.* 2015). Monitoring allows mapping the spatial and temporal development of lava domes and determining the morphological changes during the growth as well as the changes in the lava volume over time. Since 1998 seismic and other types of geophysical and geodetic monitoring at Volcán de Colima, Mexico, revealed several lava dome-building episodes of different duration from days to several years (Zobin & Tellez 2019). According to Zobin *et al.* (2017), one of the longest dome-building episodes at the volcano occurred from early 2007 until late 2009. Camera images (Fig. 1) outline the morphology of the growing lava dome at Volcán de Colima for several years (Bretón-González *et al.* 2013). The observed morphological shapes of the lava dome help to constrain the results of numerical modelling by fitting the modelled dome shapes to the observed shapes.

Analogue and numerical models play an essential role in understanding lava extrusion dynamics (e.g. Fink & Griffiths 1998; Cordonnier *et al.* 2015). Numerical models of lava dome growth help to analyse the influence of the rheological properties of magma including degassing-induced crystallization, and heat transfer on the dome morphology (e.g. Hale & Wadge 2003; Husain *et al.* 2014; Harnett *et al.* 2018; Tsepelev *et al.* 2019, 2020; Starodubtseva *et al.* 2021; Zeinalova *et al.* 2021). Numerical models of a rapid dome-building process at Volcán de Colima in 2013 have been developed by Walter *et al.* (2019) and Tsepelev *et al.* (2021). Zeinalova *et al.* (2021) developed a numerical model of a slow lava dome-building process at Volcán de Colima to analyse the influence of the magma viscosity and discharge rates on the dome growth during 2007–2009. Their viscosity model incorporated the crystal-dependent viscosity and the constant crystal-free melt viscosity, while the model did not depend on temperature. By introducing an artificial thin carapace of a high viscosity at the interface between the lava dome and the air, Zeinalova *et al.* (2021) showed that this carapace helps to constrain a lateral advancement of the lava dome and keeps the model results in a good agreement with the observation. The model by Zeinalova *et al.* (2021) does not consider thermal effects on the lava dome growth and hence does not allow a carapace to be formed and evolved due to cooling.

Here, we present a numerical study of the thermomechanical evolution of the lava dome at Volcán de Colima during 2007–2009 to understand the lava dome extrusion dynamics and the dome growth using a more sophisticated model. The research questions we try to answer in this study include: How does temperature influence the lava dynamics and the evolution of the dome carapace? How do the latent heat of crystallization and the viscous dissipation impact the lava dome dynamics? How do the thermal boundary conditions and the heat transfer at the lava–air interface influence the dome dynamics and its morphology? Below we introduce a thermomechanical model of lava dome extrusion dynamics and the dome growth (in Section 2), present the results of numerical experiments with varying physical characteristics of the lava dome (in Section 3) and discuss the results (in Section 4).

2 MODEL DESCRIPTION

2.1. Geometry and governing equations

We model a lava dome growth in a 2-D domain $\Omega = \Omega_1 \cup \Omega_2 \subset \mathbb{R}^2$. The geometry of the domain (Fig. 2) is asymmetric with respect to the model conduit. We choose one of the model geometries used by Zeinalova *et al.* (2021), allowing the horizontal spreading of the modelled lava dome to be in a good agreement with the lava dome spreading at Volcán de Colima across the E–W profile. The lava dome base is assumed to be located 20 m below the central part of the visible crater's rim (Bretón-González *et al.* 2013), the width of the crater is 257 m and the width and the depth of the conduit are 14.5 and 30 m, respectively (Zobin *et al.* 2015). The model 'conduit' is assumed to be a near-surface vertical channel filled with old, solidified rocks; fresh magma (with the prescribed temperature, crystal content and discharge rate) enters through the bottom of the channel, moves up and extrudes to the surface. In contrast to the work of Husain *et al.* (2018), we separate the model of magma extrusion and lava dome growth from the model of magma flow in a volcanic conduit and concentrate in this study on the physical processes within the growing lava dome.

In model domain Ω, we consider a 2-D incompressible, two-phase, immiscible viscous fluid flow approximating an extrusion of the lava (one fluid phase) into the air (another fluid phase) on the surface of the crater. The interface between the lava and the air presents a stress-free surface. The influence of the air phase on the lava dome growth is insignificant due to a large ratio between densities/viscosities of the air and the lava. The lava dynamics is described by the Navier–Stokes equations with the initial condition $\mathbf{u}(t = 0, \mathbf{x}) = 0$

$$\frac{\partial(\rho\mathbf{u})}{\partial t} + \langle \mathbf{u}, \nabla \rangle (\rho\mathbf{u}) - \nabla \cdot \left(\eta \left(\nabla\mathbf{u} + \nabla\mathbf{u}^T\right)\right) = -\nabla p - \rho\mathbf{g}, \quad (1)$$

the continuity equation

$$\nabla \cdot \mathbf{u} = 0, \quad (2)$$

and the heat equation with the initial condition for the temperature $T(t = 0, \mathbf{x}) = T_{\mathrm{cr}}$ for $\mathbf{x} \in \Omega_1$ and $T(t = 0, \mathbf{x}) = T_a$ for $\mathbf{x} \in \Omega_2$

$$\frac{\partial(c\rho T)}{\partial t} + \nabla \cdot (\mathbf{u}(c\rho T)) = \nabla \cdot (k\nabla T) + LH - HF + VD. \quad (3)$$

Here, t is the time; $\mathbf{x} = (x_1, x_2)$ is the position vector in 2-D Cartesian coordinates; $\mathbf{u} = (u_1, u_2)$ is the velocity; p is the pressure; $\mathbf{g} = (0, g)$, g is the acceleration due to gravity and T is the temperature. The term $LH = L^*\rho_l \frac{\mathrm{d}\phi}{\mathrm{d}t}$ describes the latent heat release in magma/lava due to crystallization (Kirkpatrick 1976; Costa *et al.* 2007a), where L^* (=3.5 × 10^5 J kg^{-1}; Costa *et al.* 2007a) is the latent heat of crystallization; ϕ is the volume fraction of crystals; and $\frac{\mathrm{d}\phi}{\mathrm{d}t} \equiv \frac{\partial\phi}{\partial t} + \nabla \cdot (\phi\mathbf{u})$. The term HF accounts for either the convective heat transfer at the interface of the lava and the air $HF_l = [\lambda(T - T_a)]\delta_s$ or the radiative and non-linear convective heat transfer at the interface $HF_n = [\varepsilon\sigma(T^4 - T_a^4) + \tilde{\lambda}(T - T_a)^{4/3}]\delta_s$ (Neri 1998; Tsepelev *et al.* 2019), where λ is the convective heat transfer coefficient, ε (=0.9; Ramsey *et al.* 2019) is the effective emissivity of the lava dome solid surface; σ is the Stefan–Boltzmann constant; $\tilde{\lambda}$ is the non-linear convective heat transfer coefficient measured in [W m^{-2} $\mathrm{K}^{-4/3}$] (Neri 1998); T_a is the air temperature; δ_s is the special function determined at interface S between the lava and the air measured in [m^{-1}]. The term $VD = \eta(\nabla\mathbf{u} + \nabla\mathbf{u}^T) : \nabla\mathbf{u}$ describes the viscous dissipation. Symbols $\nabla$is the gradient operator, $\nabla\cdot$ is the divergence operator, $^{\mathrm{T}}$ is the transposed matrix, : is

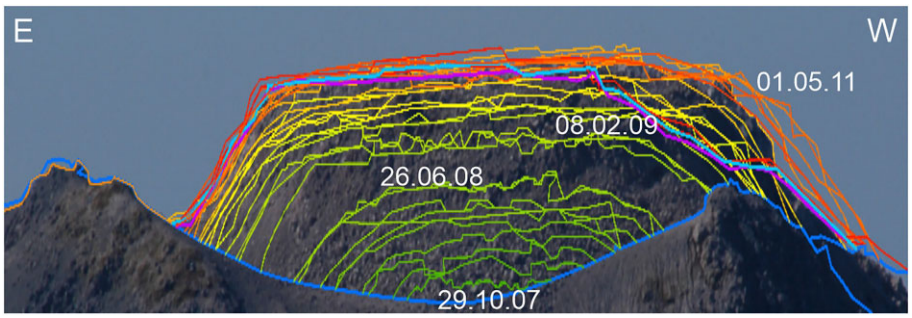

Figure 1. The lava dome at andesitic stratovolcano Volcán de Colima (based on Bretón-González *et al.* 2013). The coloured outlines of the growing lava dome along the E–W profile over the rim of the volcano crater (the blue curve) present the morphological shapes of the dome for 29 October 2007 to 5 May 2009 (greenish colours), 1 June 2009 to 1 January 2010 (yellowish colours) and 22 March 2010 to 1 May 2011 (brownish colours). The cyan and purple outlines present the morphology of the lava dome on 14 July 2011 and 21 April 2012. The dome outlines are interpreted from a sequence of camera images overlaid on one particular frame.

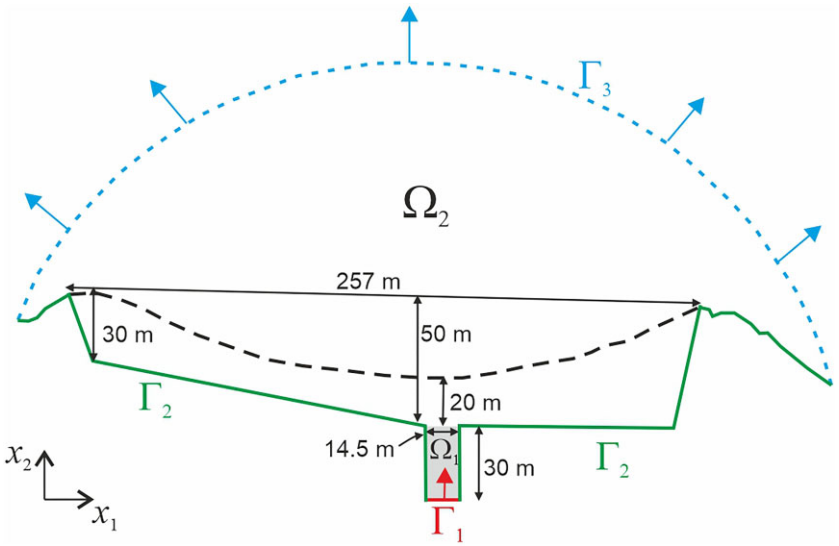

Figure 2. Sketch of the model domain. The model conduit (subdomain Ω_1) is filled by an older magma (grey-shaded), and the red arrow indicates the direction of the rise of new magma through Γ_1 (the red line) within the conduit. The green bold line Γ_2 marks the lava dome base, and the black dashed curve presents the visible crater's rim. The blue dashed curve (Γ_3) illustrates the upper boundary of the domain, through which the air escapes from the model, and blue arrows show the direction of the escape.

the double-dot product (the trace of the inner product) of two matrices and $\langle \cdot, \cdot \rangle$ is the scalar product of vectors, respectively. The model density ρ, viscosity η, thermal conductivity k and specific heat capacity c are represented as

$$\rho(t, \mathbf{x}) = \rho_l \alpha(t, \mathbf{x}) + \rho_a (1 - \alpha(t, \mathbf{x})), \quad (4)$$
$$\eta(t, \mathbf{x}) = \eta_l \alpha(t, \mathbf{x}) + \eta_a (1 - \alpha(t, \mathbf{x})),$$

$$k(t, \mathbf{x}) = k_l \alpha(t, \mathbf{x}) + k_a (1 - \alpha(t, \mathbf{x})), \quad (5)$$
$$c(t, \mathbf{x}) = c_l \alpha(t, \mathbf{x}) + c_a (1 - \alpha(t, \mathbf{x})),$$

where ρ_a, η_a, k_a and c_a are the air density, viscosity, thermal conductivity and specific heat capacity, respectively (we consider these parameters to be constant); and ρ_l, η_l, k_l and c_l are the lava density, viscosity, thermal conductivity and specific heat capacity, respectively (these parameters are not constant and may depend on the temperature, volume fraction of crystals and other physical variables; to be specified below). The function $\alpha(t, \mathbf{x})$ equals 1 for the lava and 0 for the air at each point $\mathbf{x}$ and at time t, and this function is transported with the velocity $\mathbf{u}$ according to the advection equation with the initial condition $\alpha(t = 0, \mathbf{x}) = 1$ for $\mathbf{x} \in \Omega_1$ and $\alpha(t = 0, \mathbf{x}) = 0$ for $\mathbf{x} \in \Omega_2$

$$\frac{\partial \alpha}{\partial t} + \nabla \cdot (\alpha \mathbf{u}) = 0. \quad (6)$$

2.2. Lava rheology

The lava viscosity η_l measured in [Pa s] is defined here as a multiplication of the melt viscosity η_{mt} and the relative viscosity, depending on the volume fraction of crystals η_{cr}:

$$\eta_l(T, \phi) = \eta_{\mathrm{mt}}(T) \eta_{\mathrm{cr}}(\phi). \quad (7)$$

The melt viscosity $\eta_{\mathrm{mt}}(T)$ (measured in [Pa s]) experimentally determined for lavas at Volcán de Colima is presented by the Vogel–Fulcher–Tammann equation:

$$\log_{10} \eta_{\mathrm{mt}}(T_C) = a + \frac{b}{T_C - T_g}, \quad (8)$$

where the melt viscosity was fitted for the temperatures from 1000 °C down to the glass transition temperature ($T_g = 710$ °C)

for a strain rate of one, $a = 0.29$, $b = 606.9$ °C, T_C is the temperature in °C (Lavallée *et al.* 2012). We adopt the model proposed by Costa *et al.* (2009) to define the dimensionless viscosity depending on the volume fraction of crystals as

$$\eta_{cr}(\phi) = \left(1 + \varphi^{\delta}\right)\left[1 - (1-\xi)\mathrm{erf}\left(\frac{\sqrt{\pi}}{2(1-\xi)}\varphi(1+\varphi^{\gamma})\right)\right]^{-B\phi_*}, \tag{9}$$

where $\varphi = \phi/\phi_*$; ϕ_* is the specific volume fraction of crystals representing the critical solid fraction at the onset of the exponential increase of $\eta_{cr}(\phi)$ (Costa *et al.* 2009); B is the theoretical value of the Einstein coefficient; δ, ξ and γ are the rheological parameters (Lejeune & Richet 1995; Costa *et al.* 2009). Although the crystal-dependent viscosity is influenced by the shape, size and orientation of crystals (Cimarelli *et al.* 2011; Frontoni *et al.* 2022), we do not use the dependence because of the lack of information on the crystal characteristics for the lavas from Volcán de Colima erupted from 2007 to 2009. As the crystal-bearing melt viscosity for lava samples from Volcán de Colima was estimated to be $10^{11.28}$ Pa s (Lavallée *et al.* 2007), we limit the lava viscosity η_l to a value of 10^{12} Pa s in all numerical experiments except two, where the effect of the higher viscosity (up to 10^{14} Pa s) of the lava dome carapace is analysed.

In the modelling, the volume fraction of crystals is determined from the evolutionary equation describing the simplified crystal content growth kinetics of degassing-induced crystallization (e.g. La Spina *et al.* 2016; Tsepelev *et al.* 2020)

$$\frac{\mathrm{d}\phi}{\mathrm{d}t} = -\frac{\phi - \phi_{eq}}{\tau}, \tag{10}$$

with the initial condition $\phi(t = 0, \mathbf{x}) = \phi_{cr}$ for $\mathbf{x} \in \Omega_1$ and $\phi(t = 0, \mathbf{x}) = 0$ for $\mathbf{x} \in \Omega_2$. Here, ϕ_{eq} is the volume fraction of crystals at the equilibrium state depending on the concentration of water dissolved in magma and temperature (Riker *et al.* 2015; Cashman 2020); and τ is the relaxation time (the characteristic time of the crystal content growth needed by crystals to reach ϕ_{eq}), which is required to reduce the difference between the actual (ϕ) and equilibrium (ϕ_{eq}) values of the volume fractions of crystals by a factor of e with respect to the initial difference ($\phi_{in} - \phi_{eq}$), where ϕ_{in} is the initial volume fraction of crystals in the magma. In the modelling, we assume ϕ_{eq} to be either a constant or temperature-dependent variable. The constant $\phi_{eq} = 0.83$ describes a hyperconcentrated regime of a magma/lava flow with the strong interaction of crystals and the considerable increase of the viscosity (e.g. Costa 2005; Frontoni *et al.* 2022). The temperature-dependent ϕ_{eq} was determined from laboratory measurements of Volcán de Colima lava samples at various temperatures (Moore & Carmichael 1998) by fitting parameters a_1, b_1 and c_1 to get the following relationship:

$$\phi_{eq} = 1/\left(1 + \exp\left[a_1 + b_1 T_C/T_{sp} + c_1 (T_C/T_{sp})^2\right]\right), \tag{11}$$

where $T_{sp} = 1000$ °C, $a_1 = -42.4$, $b_1 = 51.04$ and $c_1 = -11.11$.

2.3. Initial and boundary conditions

At the initial time, the model conduit (subdomain Ω_1) is filled by a lava with the volume fraction of crystals ϕ_{ct} at temperature T_{ct} and the subdomain Ω_2 by air at temperature T_a. The following conditions are imposed on the model boundary $\Gamma = \Gamma_1 \cup \Gamma_2 \cup \Gamma_3$ (Fig. 2), where Γ_1 is the part of the boundary from where new magma enters into the model via conduit; Γ_2 is the part of the boundary related to the crater surface and its nearby surrounding; and Γ_3 is the upper boundary of the model domain, through which the air escapes from the model. A new magma (of the density ρ_l, the viscosity η_l, the volume fraction of crystals $\phi = \phi_{in}$ and the temperature T_{in}) enters into the model domain at the specified extrusion rate $\mathbf{u}_{ext} = (0, u_{ext})$ through Γ_1 (red line). The initial volume fraction of crystals ϕ_{in} is taken to be 0.4 as the critical crystal fraction separating the diluted (non-interacting suspended particles) and particle-concentrated regimes of magma/lava flow (Lejeune & Richet 1995; Frontoni *et al.* 2022). Although ϕ_{in} is constant in the model, we test a sensitivity of the model with respect to a higher value of the initial volume fraction of crystals.

The lava extrusion rate (m s^{-1}) is derived from the discharge rate (m^3 s^{-1}) constraining it by optimization of the fit between the 2-D morphological shape of the observed dome (Bretón-González *et al.* 2013) and that of the modelled domes (Zeinalova *et al.* 2021). To match the observed and modelled heights of the lava dome, the following extrusion rates $\mathbf{u}_{ext}$ have been chosen following Zeinalova *et al.* (2021): 5×10^{-6} m s^{-1} for the first 300 d, 7.5×10^{-6} m s^{-1} from day 301 to day 455, 2×10^{-5} m s^{-1} from day 456 to day 480 and 1.7×10^{-5} until day 822.

The conditions imposed on the model boundary Γ_1 are simplified; namely, constant (time-independent) values of density, viscosity, the volume fraction of crystals, temperature and the extrusion rate can be considered as approximations to the dynamic conditions in a volcanic conduit. A proper coupling between the conduit and the lava dome (using dynamic conditions on the boundary) may result in a cyclic behaviour of lava dome growth (e.g. Costa *et al.* 2012).

No-slip condition $\mathbf{u} = 0$ is prescribed at Γ_2. To satisfy the incompressibility condition (eq. 2) due to lava extrusion and hence to preserve the volume of the model domain, the air should be removed from the domain at the lava discharge rate. Hence, the outflow condition is determined at Γ_3 (the blue curve) as $\mathbf{u}_{out} = u_{out}\mathbf{n}$, $\phi = 0$ and $\alpha = 0$, where $u_{out} = -|\Gamma_3|^{-1} \int_{\Gamma_1} \langle \mathbf{u}_{ext}, \mathbf{n} \rangle \mathrm{d}\Gamma$, and $\mathbf{n}$ is the outward unit normal vector at a point on the model boundary.

2.4. Solution method

To solve numerically the problem described above, we use the Ansys Fluent software (Ansys Fluent 2021R2; https://www.ansys.com/products/fluids/ansys-fluent), where the finite volume method (e.g. Ismail-Zadeh & Tackley 2010) is used to solve the models of lava dome dynamics on multiprocessor computers by numerical simulations of multi-phase viscous fluid flow and heat transfer. The software uses the volume of fluid (VOF) method (Hirt & Nichols 1981), which allows for computationally inexpensive treatment of a moving interface between two fluid phases, for example the lava and the air. The model domain is discretized by about 60 000 cells (finite volumes), and the linear size of the cells is about 0.8 m. A finer spatial discretization of the model domain slightly refines the numerical results but significantly increases the time of computations. The cells containing the interface between the lava and the air have α values between zero and unity depending on the lava proportion in the cells. The term *HF* in eq. (3) containing the special function (the Dirac delta function) is calculated in a thin layer of the cells adjacent to the interface between the lava and the air, and the special function is approximated by the ratio of the length of a relevant cell to the cell's area.

Following Zeinalova *et al.* (2021), the second-order upwind schemes are used to approximate the Laplacians, and the monotonic schemes are used to discretize convective terms in the equations. The *P*-**u** coupling is handled by the SIMPLE method (Patankar & Spalding 1972), where the relaxation parameters are chosen to be

0.01 and 0.3 for P and $\mathbf{u}$, respectively. We assign 0.5 to the relaxation parameters for α, T and ϕ. A time step is chosen in the range of 1–40 s depending on the stability and optimization of the numerical solution to assure a convergence of a set of linear algebraic equations (SLAE), which is obtained after the discretization of the governing equations. In the modelling, we use the conjugate-gradient method to solve SLAE.

A second-order implicit time integration scheme is used to solve the numerical problem. To test the stability of the numerical solution of the problem, several tests have been performed at different relaxation parameters and time steps. We note that the implicit scheme is unconditionally stable with respect to the size of time steps. An employment of explicit schemes in the model led to unstable numerical results even for the small Courant number (Courant *et al.* 1928). The high viscosity ratio between the lava and the air presents some computational challenges at their interface. Although the implicit time integration scheme used in this modelling allows for any time step size, the large time steps lead to a high numerical diffusion at the lava–air interface and to the physically implausible results; therefore, the time step was chosen sufficiently small. Also, because of the viscosity discontinuity at the lava–air interface the choice of the relaxation parameters in the SIMPLE method is critical, and sometimes the parameters were lowered to ensure the solution's stability. The numerical accuracy attains 10^{-3} for the solution of the SLAE to find P and $\mathbf{u}$, and 10^{-6} for the solution of SLAE to find α, T and ϕ.

Numerical experiments were carried out on the multiprocessor computer (bwHPC) of the Karlsruhe Institute of Technology. The time of computations of the numerical models depends on several factors including the complexity of the mathematical problem, the number of computational cells, the number of cores and the time-step size. For example, 1 d of the lava dome growth in the model (eqs 1–10 with the initial and boundary conditions described in Section 2.3) is computed by eight cores for about 6 min, using the model time step 40 s. Figs 3–5, 7–8, 10–11 were made with ParaView visualisation software (version 5.9.0-RC3 64-bit, https://www.paraview.org).

3 NUMERICAL RESULTS

Here, we present the results of numerical experiments analysing the influence of the following thermal conditions on the dome growth and its morphology: (i) the heat transfer at the interface between the lava and the air, (ii) the latent heat release during crystallization, (iii) the viscous dissipation, (iv) the temperature-dependence of the volume fraction of crystal at the equilibrium state and (v) the heat transfer at the interface between the lava and the conduit wall/the crater. Finally, we use the model to study the lava dome growth during the 2007–2009 dome-building eruption at Volcán de Colima. The principal purpose of this analysis is to understand how the thermal conditions (i)–(v) influence the dome evolution individually and in combination, and which of the conditions influence the model results most significantly. Eqs (1)–(11) have been used to solve the models of lava dome growth. The numerical experiments are described in Table 1, and the model parameters used in the experiments are listed in Table 2. The first and second sets of numerical experiments concern the influence of the convective (described in Section 3.1) and convective-radiative (Section 3.2) heat flux at the lava–air interface on the morphology of modelled lava domes, when the latent heat release during crystallization, the viscous dissipation and the temperature-dependent volume fraction of crystals are accounted. The third set of experiments (Section 3.3) consider the effects of various thermal conditions at the conduit wall and the crater surface and the fourth set of two experiments (Section 3.4) deal with the evolution of the lava dome at Volcán de Colima for several years.

3.1. Convective heat transfer at the lava–air interface

In the case of the convective heat transfer at the interface between the lava and the air ($HF = HF_l$ in eq. 3), we study the lava dome growth with no latent heat ($LH = 0$) and no viscous dissipation ($VD = 0$) terms in the heat equation (eq. 3; experiment 1.1), with the added VD term (experiment 1.2), the added LH term and constant $\phi_{\rm eq}$ (experiment 1.3) and the added LH term and the temperature-dependent $\phi_{\rm eq}$ as defined in eq. (11; experiment 1.4). The results of the numerical experiments, namely, the temperature, crystal content, viscosity and flow velocity at day 300 are presented in Fig. 3.

The dome in these experiments builds upward and advances horizontally with a higher velocity towards the right due to the crater's geometry chosen in the model. The magma at temperature 1250 K enters the model conduit and extrudes on the surface forming a lava dome. This temperature is in a good agreement with the temperatures of dome-building eruptions at Volcán de Colima (Lavallée *et al.* 2008). The convective heat transfer at the interface between the lava and the air results in a temperature decrease and in the development of a cold surface layer of the lava dome (carapace). In the dome interior, the lava remains hot enough and less viscous, and hence behaves as a ductile and mobile material throughout the entire period of the dome growth. This occurs because the thin dome carapace is unable to restrain the less viscous lava in the dome interior.

As the characteristic time of the crystal content growth τ is chosen to be 5 d, crystals reach their equilibrium state rapidly already within the conduit, and the volume fraction of crystals stays constant (=0.83) in the lava dome after that (see Fig. 3, experiments 1.1–1.3). The smaller the relaxation time, the faster the crystallization process converges to its equilibrium state, the lava viscosity increases and the more viscous lava builds dome rather vertically than horizontally (e.g. Tsepelev *et al.* 2020; Zeinalova *et al.* 2021). The crystal-dependent viscosity reaches the value $\eta_{\rm cr}(\phi = 0.83) \sim 10^6$, and hence, the dynamics of the lava dome depends on the temperature and the melt viscosity.

The dynamics of magma flows in a long narrow conduit is controlled by thermal effects due to heat generation by the viscous dissipation; namely, the dissipation leads to a temperature rise during the magma ascent in the conduit (Costa *et al.* 2007b). In experiment 1.2, we have investigated the influence of the viscous dissipation on the lava dome development. We found that the effect of the heat generation due to the viscous dissipation is negligible, because the shear rates are much smaller than those in the narrow conduit; the temperature change is within a degree compared to the case of experiment 1.1 (see Supporting Information, SM). This leads to almost invisible change in lava viscosity and the morphological shape of the dome (see Fig. 3, experiment 1.2).

The latent heat of crystallization is a part of the entire heat budget of the thermal history of lava domes. The latent heat released during the crystallization influences the conduit and lava dome temperature and contributes to variations in the lava viscosity (Hale *et al.* 2007; Costa *et al.* 2007a; Morse 2011). In experiment 1.3, we have analysed the influence of the latent heat on the lava dome temperature

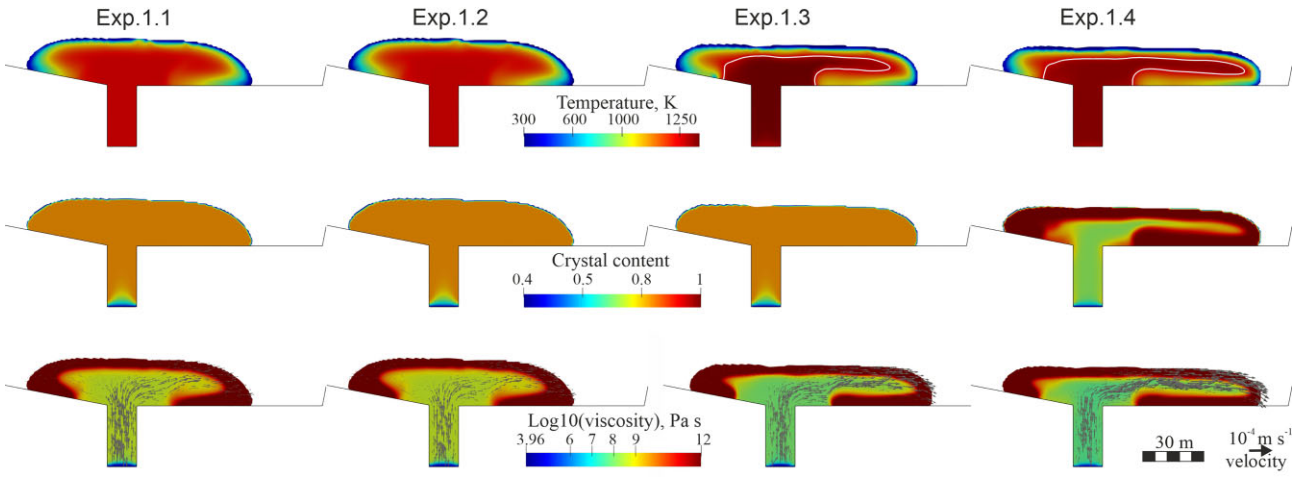

Figure 3. Modelled lava dome growth presenting the temperature, crystal content and viscosity together with the velocity vectors for the convective heat transfer at the lava–air interface at time $t = 300$ d. The white curves (here and in Fig. 5) represent the area of the elevated temperature due to the latent heat release.

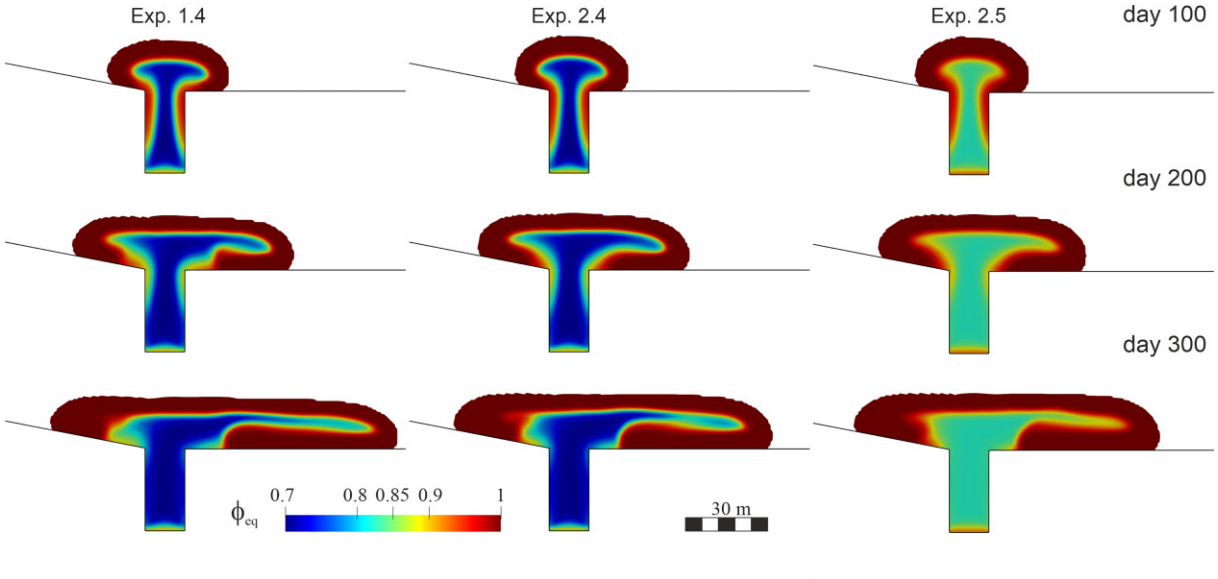

Figure 4. The evolution of the temperature-dependent volume fraction of crystals at the equilibrium state at times of 100, 200 and 300 d.

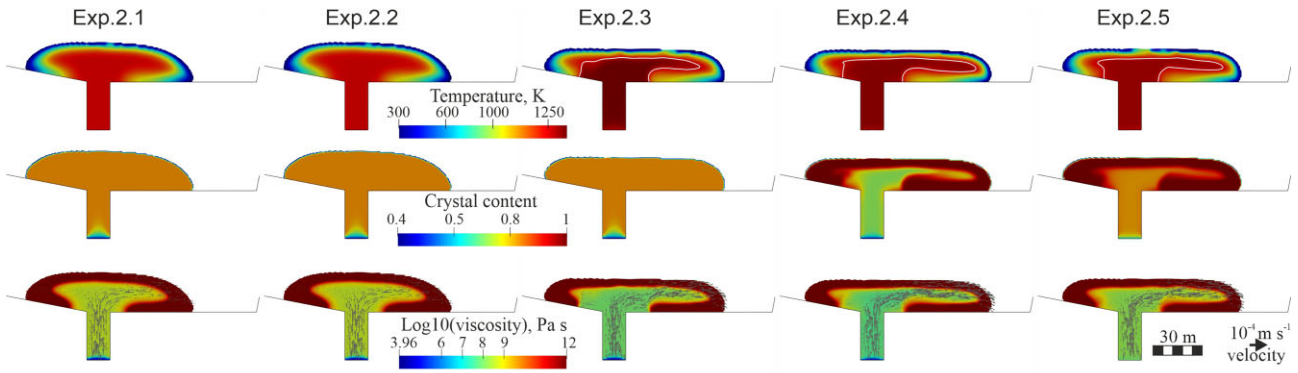

Figure 5. Modelled lava dome growth presenting the temperature, crystal content and viscosity together with the velocity vectors for the convective radiative heat transfer at the lava–air interface at time $t = 300$ d.

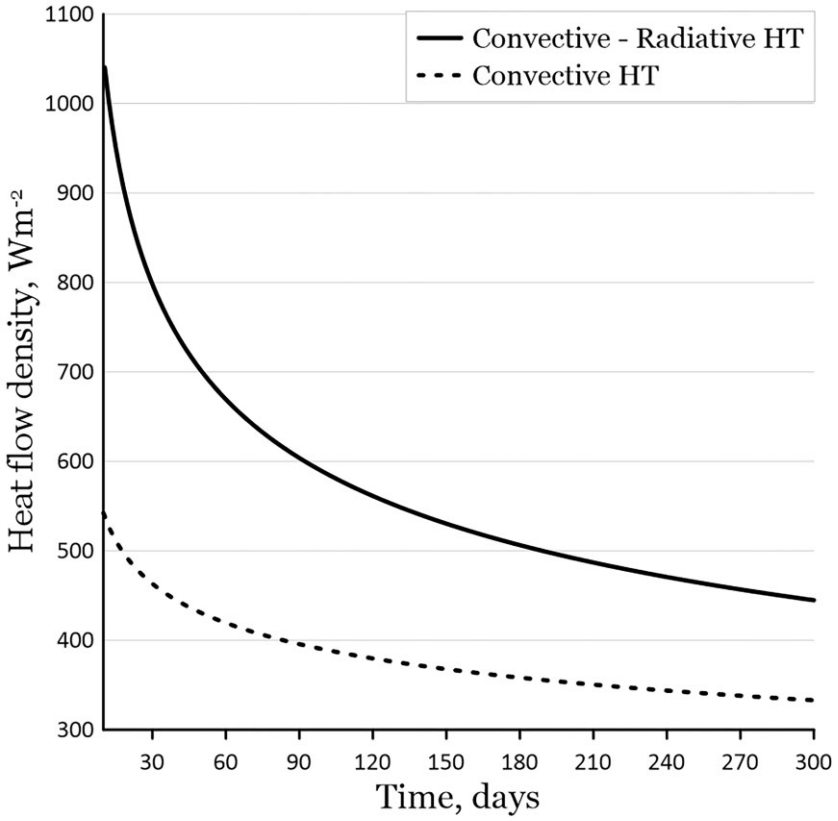

Figure 6. Heat flow density calculated for convective (dashed curve) and non-linear convective and radiative (bold curve) heat transfer (HT). At each time step, the heat flow density presents the average value of the densities calculated over each cell of the lava–air interface. The average density data for 300 d has been smoothed by a power-law fit.

and its viscosity. Due to a convective heat loss at the lava–air interface, the high-viscous carapace develops. The temperature increases in the dome interior from 1250 to 1367 K due to the latent heat release (Fig. 3, experiment 1.3; the area of the elevated temperature is marked by a white curve) compared to the case with no latent heat (Fig. 3, experiment 1.1). The higher temperature within the dome interior promotes dome flattening and its lateral advancement to the right compared to that without the latent heat transfer.

When the volume fraction of crystals depends on temperature (experiment 1.4), the release of the latent heat postpones the crystallization, this lowers slightly the lava viscosity, and it results in a further flattening of the lava dome and its horizontal advancement (Fig. 3, experiment 1.4). In experiment 1.4, all parameters are the same as in experiment 1.3 except $\phi_{eq}(T)$, which is now a temperature-dependent variable. The equilibrium value $\phi_{eq}(T)$ decreases to about 0.7 due to the increased temperature as a result of the latent heat release (Fig. 4). The maximum temperature of the modelled lava dome drops to the value of 1329 K compared to the maximum temperature of 1367 K in the case of experiment 1.3; this is associated with the reduction in $\phi_{eq}(T)$ and the subsequent decrease of the latent heat release. The crystal content becomes lower, while the lava viscosity in the dome interior slightly decreases to about $10^{7.5}$ Pa s in the right overhang of the lava dome. This leads to a minor increase in the flow velocity and the lava dome advances to the right more than in the case of experiment 1.3; the height of the dome decreases accordingly. Despite the viscosity of the carapace is higher compared to that of the dome interior, it cannot restrict the horizontal flow. We note that although the temperature-dependence of the crystal content (eq. 11) might be plausible for the use in lava dome modelling, it raises uncertainties about being a well-parametrized representation for high-silica magmas at temperatures lower than 1250 K (e.g. Moore & Carmichael 1998).

The difference between the shapes of the modelled domes in experiments 1.1–1.2 and in experiments 1.3–1.4 is associated with the distribution of the lava viscosity in the dome interior. A higher viscosity of the lava dome interior (experiments 1.1–1.2) is required to maintain a vertical growth. The lava dome (experiments 1.3–1.4) tends to flatten due to its lower viscosity in the dome interior (ranging from about $10^{8.7–9.3}$ Pa s to 10^{10} Pa s) compared to the viscosity of the dome interior in the case of experiment 1.1 or experiment 1.2 (ranging from about $10^{10.3}$ Pa s to about $10^{11.8}$ Pa s).

3.2. Non-linear convective and radiative heat transfer at the lava–air interface

We present here the results of numerical experiments on the lava dome growth accounting for non-linear convective and radiative heat transfer ($HF = HF_n$ in eq. 3) at the interface between the lava and the air. As in the previous case (Section 3.1), we study models of the lava dome growth with no latent heat and no viscous dissipation accounted (experiment 2.1), with the viscous dissipation term (experiment 2.2) and the latent heat term (experiment 2.3). Also, we analyse the influence of the temperature-dependent ϕ_{eq} (experiment 2.4) and the initial volume fraction of crystals ϕ_{in} (experiment 2.5) on the lava dome morphology.

A thick carapace forms at the lava–air interface due to the non-linear convective-radiative heat flux. The thicker carapace (compared to the carapace in the case of the convective heat transfer

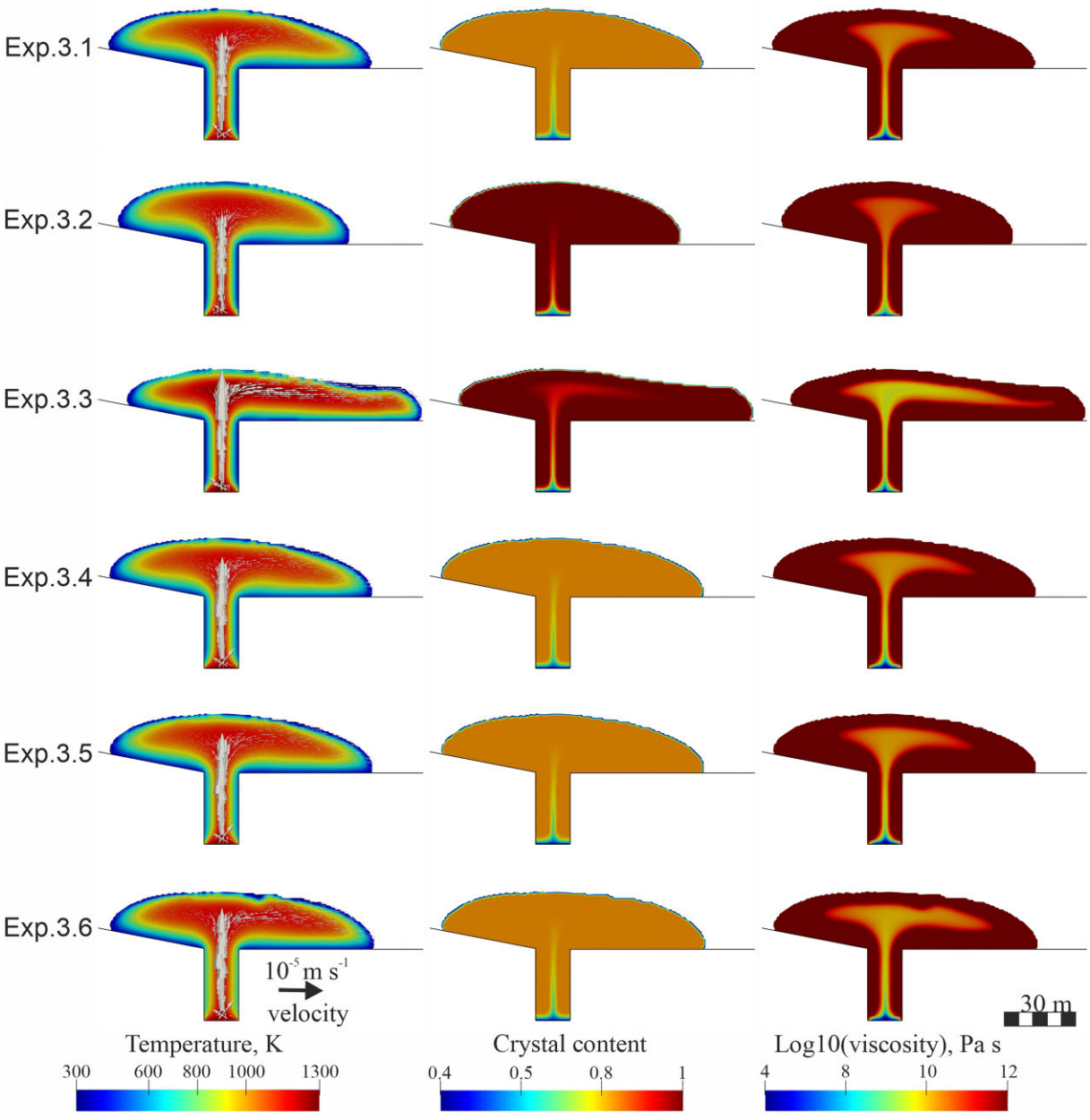

Figure 7. Modelled lava dome growth. The temperature together with the velocity vectors (left-hand column), crystal content (middle column) and viscosity (right-hand column) at time $t = 300$ d.

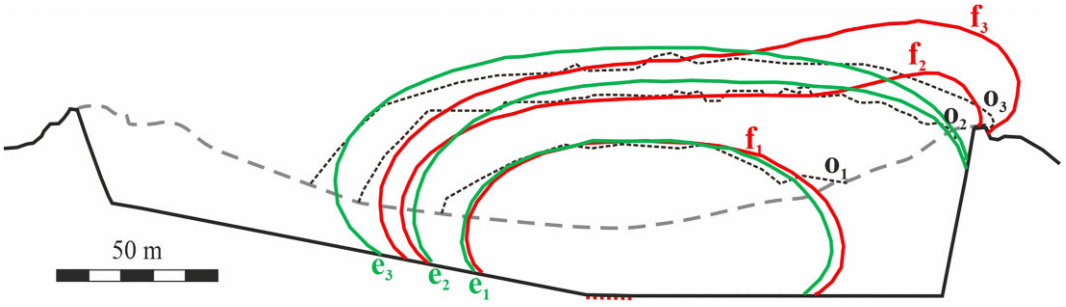

Figure 8. Comparison of the morphological shapes of the modelled domes in experiment 4.1 (solid green curves with index *e*) and experiment 4.2 (solid red curves with index *f*) alongside with the observed shapes of the lava dome (dotted black curves with index *o*) on 1 May 2008 (index 1), 4 December 2008 (index 2) and 1 April 2009 (index 3). The grey dashed line is the crater's rim. The black bold line presents the base of the crater, and the red dotted line is the top of the conduit.

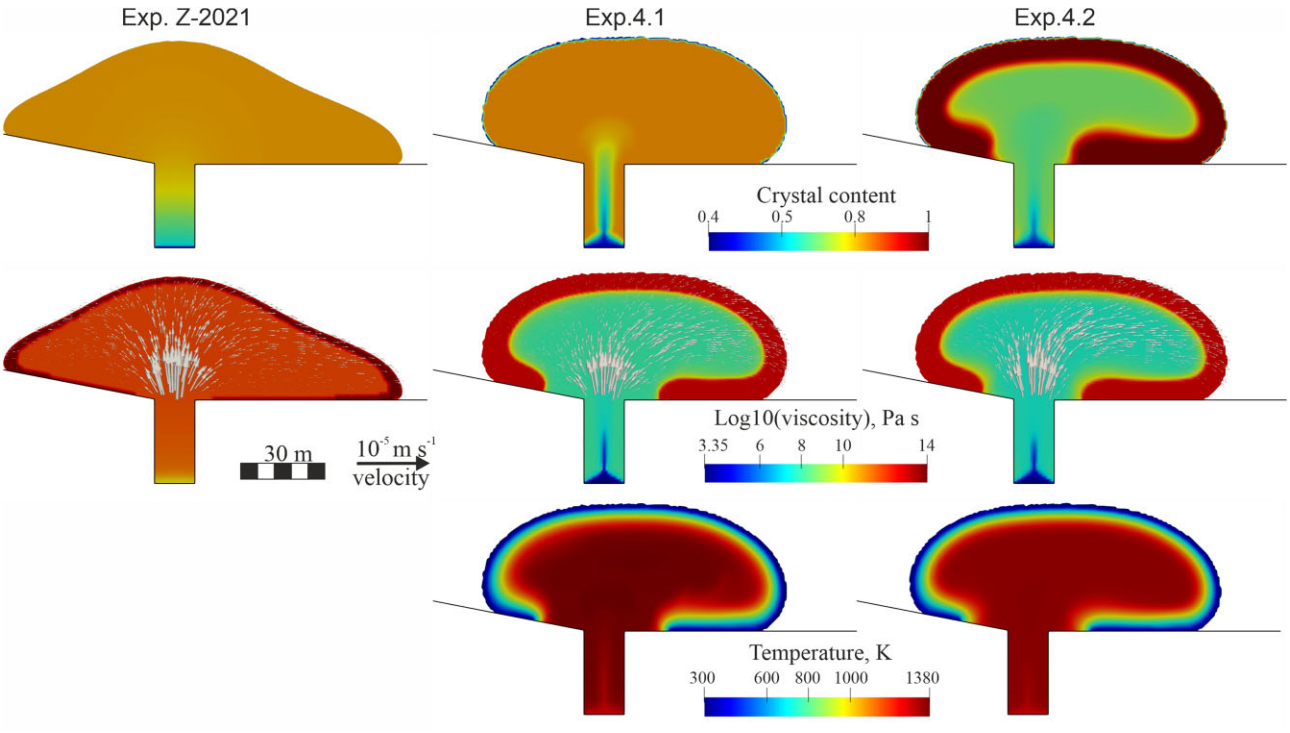

Figure 9. Comparison between three models of the lava dome growth at Volcán de Colima at time $t = 480$ d: (the left-hand panels) the crystal content and viscosity in experiment Z-2021 by Zeinalova *et al.* (2021); the crystal content, the viscosity and temperature in experiment 4.1 (the middle panels) and experiment 4.2 (the right-hand panels). The flow velocity vectors are shown in the modelled domes.

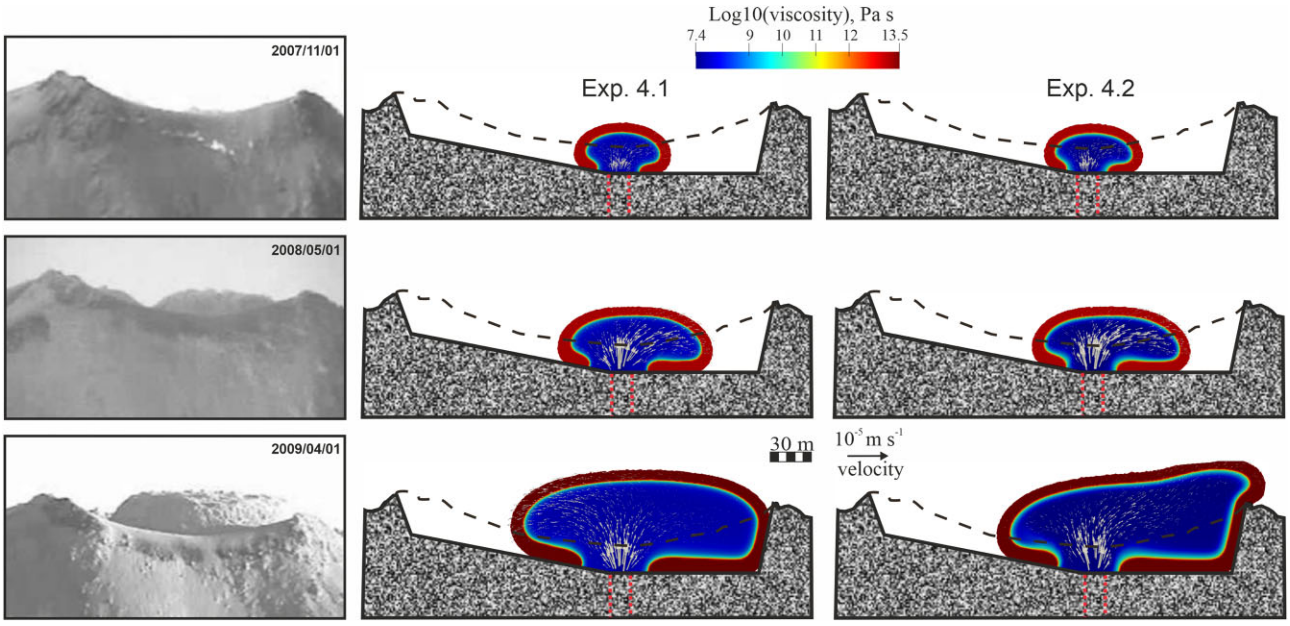

Figure 10. Images of the lava dome evolution at Volcán de Colima (left-hand column; Bretón-González *et al.* 2013) versus the modelled lava dome growth in experiment 4.1 (middle column) and experiment 4.2 (right-hand column) at times of 1 November 2007 (upper panels), 1 May 2008 (middle panels) and 1 April 2009 (lower panels). The middle and right-hand columns present the lava viscosity distribution with the flow velocity vectors. The black dashed line is the crater's rim, and the red dashed line is the position of the conduit.

only; Section 3.1) retards the horizontal advancement of the lava dome (Fig. 5) and promotes the growth of the dome upwards. The temperature and viscosity structures of the lava dome interior in experiments 2.1–2.4 are similar to those in experiments 1.1–1.4.

To analyse the influence of the initial volume fraction of crystals ϕ_{in} on morphology of lava dome, ϕ_{in} has been increased (from 0.4 to 0.6) in experiment 2.5. Since the initial volume fraction of crystals in experiment 2.5 is higher compared to experiment 2.4, the temperature decreases for about 20 K due to a smaller latent heat release. The lower temperature results in a higher value for $\phi_{eq} \sim 0.83$ (Fig. 4, experiment 2.5) in contrast to experiment 2.4, where $\phi_{eq} \sim 0.73$ (Fig. 4, experiment 2.4). This leads to a

Table 1. Numerical experiments.

No. exp.	Convective heat transfer	Convective-radiative heat transfer	Latent heat release	Viscous dissipation	Thermal conditions at the model boundary	ϕ_{eq}/ϕ_{in}
1.1	✓				Heat flux = 0	0.83/0.4
1.2	✓			✓	Heat flux = 0	0.83/0.4
1.3	✓		✓		Heat flux = 0	0.83/0.4
1.4	✓		✓		Heat flux = 0	$\phi_{eq}(T)$/0.4
2.1		✓			Heat flux = 0	0.83/0.4
2.2		✓		✓	Heat flux = 0	0.83/0.4
2.3		✓	✓		Heat flux = 0	0.83/0.4
2.4		✓	✓		Heat flux = 0	$\phi_{eq}(T)$/0.4
2.5		✓	✓		Heat flux = 0	$\phi_{eq}(T)$/0.6
3.1	✓				Temperature 350 K at Γ_2	0.83/0.4
3.2	✓				Temperature 350 K at Γ_2	$\phi_{eq}(T)$/0.4
3.3	✓		✓		Temperature 350 K at Γ_2	$\phi_{eq}(T)$/0.4
3.4	✓				Conductive heat flux at Γ_2	0.83/0.4
3.5	✓				Temperature 350 K at the crater surface, 500 K at the conduit wall	0.83/0.4
3.6	✓				Temperature 350 K at the crater surface, 700 K at the conduit wall	0.83/0.4
4.1		✓	✓	✓	Heat flux = 0	0.83/0.4
4.2		✓	✓	✓	Heat flux = 0	$\phi_{eq}(T)$/0.4

Table 2. Model parameters and their values.

Symbol	Parameter, unit	Value
B	the Einstein coefficient (in eq. 9)	2.5
c_a	specific heat capacity of air, J kg^{-1} K^{-1}	1006
c_l	specific heat capacity of lava, J kg^{-1} K^{-1}	1200
g	acceleration due to gravity, m s^{-2}	9.81
k_a	thermal conductivity of air, J s^{-1} m^{-1} K^{-1}	0.025
k_l	thermal conductivity of lava, J s^{-1} m^{-1} K^{-1}	3.0
L^*	latent heat coefficient, J kg^{-1}	3.5×10^5
T_a	air temperature, K	300
T_{ct}	initial temperature of the magma in the conduit, K	1150
T_{in}	temperature of the new magma entering the conduit, K	1250
$\mathbf{u}_{ext}$	extrusion rate, m s^{-1}	
	from day 1 to day 300	5.0×10^{-6}
	from day 301 to day 455	7.5×10^{-6}
	from day 456 to day 480	2.0×10^{-5}
	from day 481 to day 822	1.7×10^{-5}
δ	rheological parameter (in eq. 9)	7.24
ε	effective emissivity	0.9
ϕ_{ct}	initial volume fraction of crystals in the magma in the model conduit	0.8
ϕ_{in}	volume fraction of crystals of the new magma entering the model conduit	0.4
ϕ_*	specific volume fraction of crystals	0.591
γ	rheological parameter (in eq. 9)	5.76
η_a	air viscosity, Pa s	0.001
λ	coefficient of convective heat transfer, J s^{-1} m^{-2} K^{-1}	3.0
$\tilde{\lambda}$	non-linear convective heat transfer coefficient, J s^{-1} m^{-2} K$^{-4/3}$	5.5
ρ_a	air density, kg m^{-3}	1
ρ_l	lava density, kg m^{-3}	2500
σ	Stefan–Boltzmann constant, J s^{-1} m^{-2} K^{-4}	5.67×10^{-8}
τ	characteristic time of the crystal content growth, days	5
ξ	rheological parameter (in eq. 9)	4.63×10^{-4}

slight increase of the viscosity $\sim 10^8$ compared to $\sim 10^{7.5}$ in experiment 2.4, and to a retardation in the lava advancement to the right (Fig. 5). While there are some insignificant differences in shapes of the lava dome, the internal structure of the lava dome remains relatively consistent in both experiments. Therefore, the change of the initial volume fraction of crystals by at least 0.2 does not significantly affect the dome dynamics and its morphology.

To analyse the surface heat flux in the model, we have computed the linear HF_l and non-linear HF_n heat flow density. The modelled surface heat flow density is presented in Fig. 6 in the cases of the convective heat transfer (experiment 1.1) and the non-linear convective and radiative heat transfer (experiment 2.1). The modelled surface heat fluxes decrease with time. The heat flux, inferred from infrared images obtained by airborne thermal remote sensing during the lava dome building at Volcán de Colima 2007–2010 (Hutchison *et al.* 2013), decreases with time as well. The maximum modelled surface temperature on the onset of the lava dome growth is 555 K, and the inferred temperature from the remote sensing measurements is 550–620 K for the first few days (Hutchison *et al.* 2013).

In the earlier stages of eruption, the dome temperatures were high as the cooled crust (carapace) on the dome was the thinnest, and hence the surface heat flux was the highest. The carapace becomes thicker with time, and the surface heat flux keeps the tendency to decrease while the temperature may vary on the surface during active dome building (Hutchison *et al.* 2013). Meanwhile, the heat flow densities obtained from the modelling and from the inferred temperature data (Hutchison *et al.* 2013) differ because of the different values of the convective heat flow coefficient and the effective emissivity used in the calculation of the heat flow density. Numerical experiments show that the heat exchange between the lava and the air plays a significant role in the development of the lava dome carapace during the long dome-forming eruptions.

3.3. Thermal conditions at the conduit wall and crater surface

In this section we present the results of the numerical experiments related to variations of the thermal conditions at the crater surface and the magma–rock interface. These experiments are conducted under the assumption of the convective heat transfer ($HF = HF_l$) at the interface between the lava and the air and no viscous dissipation ($VD = 0$). In experiments 3.1–3.3, the same thermal boundary condition (temperature 350 K at Γ_2, see Fig. 2) is assumed; the volume fraction of crystals at the equilibrium state is constant in experiment 3.1 and depends on the temperature in experiments 3.2 and 3.3. In addition, the latent heat due to crystallization is introduced in experiment 3.3. In the subsequent experiments (experiments 3.4–3.6), different thermal boundary conditions at the crater surface and the magma–rock interface and the constant ϕ_{eq} are used. Namely, in experiment 3.4, a conductive heat flux is assumed at Γ_2 corresponding to the wall-rock temperature $T = 350$ K, thermal conductivity 3.5 J s^{-1} kg^{-1} K^{-1} and the zero-thickness of the wall. In experiments 3.5 and 3.6, the temperature $T = 350$ K at the crater surface and the temperature $T = 500$ K at the conduit wall in case of experiment 3.5 and $T = 700$ K in experiment 3.6 are assumed. The experiments show how the different conditions affect the temperature, crystal content, viscosity and velocity in the modelled conduit and lava dome.

The inclusion of the temperature-dependent ϕ_{eq} (experiment 3.2) slightly alters the viscosity distribution, retards the lava advancement and leads to vertical growth compared to experiment 3.1 (Fig. 7). In the case of experiment 3.3, the latent heat release leads to increased temperatures, reduction of the crystal content and lowering the lava viscosity. This decrease in viscosity contributes to a horizontal advancement of the lava and flattening the lava dome (Fig. 7). The change in temperature and heat flux at boundary Γ_2 (Fig. 7, experiments 3.1–3.6) leads to cooling of the lava dome at the contact with the crater surface and with the conduit wall. The hot lava concentrates in the conduit centre, where the velocity increases. The changes in the thermal conditions at the crater surface and the conduit wall do not significantly influence the morphological shapes of the lava domes in experiments 3.1, 3.4–3.6. Meanwhile, we note that as the eruption proceeds, the heat flux from the ascending magma will gradually decrease due to heating up the surrounding rocks.

3.4. Lava dome growth at Volcán de Colima from 2007 to 2009

In this section we present the results of two numerical experiments (experiments 4.1 and 4.2) related to the lava dome growth from the start of the lava extrusion in February 2007 until April 2009. In both experiments, the numerical model includes eqs (1)-(10) with the initial and boundary conditions described in Section 2.3, assuming the non-linear convective and radiative heat transfer at the lava–air interface and including the latent heat of crystallization and the viscous dissipation (even though its effect is negligible) in eq. (3). We use the constant (experiment 4.1) and the temperature-dependent (experiment 4.2) ϕ_{eq} in the modelling.

Laboratory and numerical experiments showed earlier that cooling increases the viscosity of the uppermost part of the lava dome and results in developing a high-viscosity carapace (e.g. Fink & Griffiths 1998; Griffiths 2000; Hale & Wadge 2003; Hale *et al.* 2007; Hale 2008; Husain *et al.* 2014, 2018, 2019; Harnett *et al.* 2018; Tsepelev *et al.* 2020). As the viscosity of the model dome carapace is higher than 10^{12} Pa s at lower temperatures, the threshold of the lava viscosity (eq. 7) was raised to 10^{13} Pa s (and to $10^{13.5}$ Pa s at day 600) in both experiments. The increase of the viscosity in the carapace allows for simulating a lava dome, which morphological shape fits better the dome shape observed at Volcán de Colima. We have used several thresholds (from $10^{12.5}$ to 10^{14} Pa s) and found that the lava dome still advances horizontally at $10^{12.5}$ Pa s and develops an obelisk-type dome at 10^{14} Pa s, and both scenarios of the dome development contradict the observations on the lava dome growth at Volcán de Colima.

Zeinalova *et al.* (2021) used a similar approach but introduced an artificial thin carapace with the viscosity 10^{14} Pa s in the model of lava dome growth at day 481 after the commencement of the lava extrusion to mimic the growth of the observed lava dome, as their model did not consider thermal effects (that is, eqs 3, 5 and 8 were not used) and, hence, could not generate a high viscosity carapace. Here, we show how the carapace evolves self-consistently due to cooling of the uppermost part of the dome.

Fig. 8 presents the morphological shapes of the modelled lava dome at times of 1 May 2008 (day 480), 4 December 2008 (day 704) and 1 April 2009 (day 822). The increased viscosity of the carapace due to cooling restrains the lateral advancement of the dome. The

modelled dome develops steep flanks, and its morphology fits observations at Volcán de Colima with a few meter differences in the length of the dome.

Initially, the morphological shapes of the modelled domes (Fig. 8, green and red curves with index *e* and *f*, respectively) fit quite well the observed shape of the lava dome (black dashed curve with index *o*). Later, the lava advances to the right in experiment 4.2 compared to that in the case of experiment 4.1, and this can be associated with a decrease (to about $10^{7.5}$ Pa s) in the viscosity of the dome interior (Fig. 9). These results underscore that the variations in viscosity, particularly between the dome interior and its carapace, along with the introduction of the temperature-dependent ϕ_{eq}, influence the lava dome growth and its morphological shapes.

To quantitatively compare the morphological shape of the modelled dome with that of the observed dome (Fig. 8), we evaluate the closeness of the shape $\tilde{F}$ of the part $\tilde{L}$ of the observed dome, which is visible over the crater's rim (dotted black curves), and the shape F_i of the part L_i of the modelled dome also visible over the crater's rim. We use the quality functional J_i, which is based on the symmetric difference (Starodubtseva *et al.* 2021):

$$J_i(\tilde{F}, F_i) = \frac{S\left((\tilde{L} \cup L_i)\backslash(\tilde{L} \cap L_i)\right)}{S(\tilde{L})}, \tag{12}$$

where indices $i = 1$ and $i = 2$ denote the modelled domes in experiments 4.1 and 4.2, and S is the area measured in [m^2]. The closeness of the function J_i to zero means the closeness of the observed shape $\tilde{F}$ to the model shape F_i. The functional J_1 takes the values 0.12, 0.16 and 0.11 and the functional J_2 the values 0.12, 0.17 and 0.25 for days 480, 704 and 822, respectively. While the morphological shapes of both modelled domes fit the observed shape with the almost same accuracy for the first 704 days, the modelled shapes deviate from each other at the later stages of the dome growth. Namely, in experiment 4.2, the lava advances considerably to the right moving over the crater's rim and develops an overstepping feature, while the modelled dome heights do not fit well the height of the observed lava dome. In the case of experiment 4.1, the morphological shape of the modelled dome agrees better with the observation.

The carapace of the viscosity 10^{14} Pa s in the model by Zeinalova *et al.* (2021) (Fig. 9, experiment Z-2021) is thinner than that of the viscosity $10^{13.5}$ Pa s in the studied models (Fig. 9, experiments 4.1 and 4.2). The thicker carapace constrains the lava dome advancement despite its viscosity lower than in the case of the modelled carapace by Zeinalova *et al.* (2021). The interior of the lava domes in experiments 4.1 and 4.2 has a low viscosity ranging from about $10^{7.5–8}$ to 10^9 Pa s.

Although the volume fraction of crystals in experiment 4.1 remains relatively consistent with that in experiment Z-2021 (Zeinalova *et al.* 2021), the viscosity of the modelled dome interiors in these experiments differs significantly from each other and should influence the dome's shape. The temperature-dependent volume fraction of crystals at the equilibrium state exerts an impact on the crystal content (experiment 4.2) leading to a decrease in crystal content within the dome interior from 0.83 (Fig. 9, experiment 4.1) to 0.7 (Fig. 9, experiment 4.2). This crystal content's reduction has a corresponding effect on the latent heat release during crystallization, decreasing the temperature from 1380 K (in experiment 4.1) to 1335 K (in experiment 4.2). Meanwhile the shapes of the modelled domes (in experiments 4.1 and 4.2) remain very similar. Therefore, the viscosity and the thickness of the carapace influence more profoundly the morphological shapes of lava domes.

The modelled domes are presented in Fig. 10 together with the recorded images of the lava dome at Volcán de Colima (Bretón-González *et al.* 2013). The dome interior in both experiments remains hot and therefore ductile throughout the dome growth during the studied period of the lava extrusion.

4 DISCUSSION AND CONCLUSION

Lava dome eruptions at Volcán de Colima are episodic and vary in the dome building duration from days to months and years without explosive dome collapses. The eruption started in February 2007 with the extrusion of hot rocks from a rising plug of the older magma filling the uppermost part of the conduit (Hutchison *et al.* 2013). The dome grew continuously, and from the beginning of 2008 its morphology resembled closely that of a truncated cone (Bretón-Gonzalez *et al.* 2013; Fig. 1).

Our numerical thermomechanical models of the lava dome growth are validated against recorded dataset from Volcán de Colima during the long dome-building episode lasting from 2007 to 2009 (Bretón-Gonzalez *et al.* 2013). We show that long episodes of the dome building require a viscosity model depending on both the crystal content and the temperature to allow for generating a thermal, highly viscous carapace (e.g. Zeinalova *et al.* 2021). This numerical study has estimated the influence of the lava temperature, thermal boundary conditions, the crystal content, the latent heat of crystallization, the heat due to the viscous dissipation and the heat transfer mechanisms at the lava–air interface on the lava dome dynamics and its morphology.

Although degassing-induced crystallization plays a significant role in lava dome building process, especially during short dome-building episodes (e.g. Walter *et al.* 2019; Tsepelev *et al.* 2021; Zeinalova *et al.* 2021), we have shown that the rheological stiffening within the lava dome is essentially controlled by cooling during long dome-building episodes. Cooling influences the viscosity of the lava dome at its interface with the air making the dome carapace more viscous and promotes a development of lobe-shaped lava dome (Watts *et al.* 2002; Tsepelev *et al.* 2020). The model results indicate that a high-viscous carapace of the lava dome at Volcán de Colima retards the dome lateral advancement and promotes the development of steep slopes on the dome sides. As the magma ascent is slow during the dome growth at Volcán de Colima, the crystal content in the magma grows rapidly and the crystallinity (the volume fraction of crystals) reaches almost its equilibrium state already in the model conduit. Meanwhile, the latent heat release due to crystallization lowers the lava crystallinity.

We have demonstrated that (i) the dome carapace becomes thicker in the case of the convective-radiative heat transfer at the interface between the lava and the air; (ii) the latent heat of crystallization leads to elevated temperature in the conduit and in the lava dome interior and to further flattening of the dome; (iii) the heat source within the dome due to the viscous dissipation is negligible, and can be omitted in the modelling of the lava dome growth and (iv) thermal boundary conditions influence the magma flow pattern and the crystal content in the conduit with an insignificant impact to the dynamics of the dome interior, and hence, to the morphological shapes of the lava dome.

The dynamics of dome eruptions can be more complicated than that described in this work due to the complex interplay between magma decompression, degassing, degassing-induced crystallization, pore-fluid dynamics, temperature and rheological properties of the erupted lava (e.g. Fink & Griffiths 1998; Melnik & Sparks

1999; Calder *et al.* 2015). Particularly, our current model cannot simulate a brittle, but ductile only, behaviour of the dome carapace. Tsepelev *et al.* (2020) showed that in the case of the strain-rate dependent viscosity, the viscosity of the dome carapace increases with the decrease of the strain rate and vice versa. This dependence of the viscosity on strain rates presents a typical behaviour of a non-Newtonian Herschel–Bulkley fluid exhibiting rigid body properties at low strain rates and viscous fluid properties at higher rates.

The dome morphology shall also vary with the strain rate resulting in short and wide domes at higher strain rates, and tall and narrow domes at lower rates (Tsepelev *et al.* 2020). The form of crystals influences the lava viscosity (Frontoni *et al.* 2022) and, hence, may lead to changes in the dome morphology. Discrepancies in the shapes of the modelled dome compared to the observed dome shapes can also be associated with a brittle behaviour of the natural dome carapace and its failures, which are important components in natural lava dome developments. Furthermore, 2-D numerical models cannot capture complexity of natural lava dome growth, and 3-D models should provide additional insight into lava dome dynamics.

Although no numerical model is likely to represent the exact lava dome extrusion dynamics, the thermomechanical model accounts for the main dynamic processes and characteristics within the shallow conduit and lava dome, such as the mass and heat transfer (eqs 1–6), the degassing-induced crystallization kinetics (eq. 10), the latent heat of crystallization, the convective and radiative heat flux at the lava interface with the air, conductive heat flux at the crater surface and the shallow conduit wall, and the lava viscosity depending on the volume fraction of crystals and the temperature (eqs 7–9). The present model can be further developed by incorporating the water content and stress-dependence into the lava viscosity model, although efficient degassing, as observed during lava-building eruptions at Volcán de Colima, results in a low (about 9 per cent) mean porosity (Lavallée *et al.* 2007) and low water contents (2.5 to 0.1 wt. per cent) of Colima eruptive products (Reubi & Blundy 2008).

Using observations (i.e. morphological shapes of the lava dome at Volcán de Colima and experimentally derived material properties of lava samples from the volcano) and models (i.e. crystal growth kinetics, lava viscosity and various heat transfer), this contribution demonstrates that the lava dome growth at Volcán de Colima for 2007–2009 can be well described. Although it was known that the cooling at the interface of the lava dome and the air plays a significant role in the evolution of dome carapaces, we have shown here that the combined effects of the thermal evolution and crystallization in the dome interior and the cooling at the lava–air interface shape the lava dome during long episodes of its building. The developed thermomechanical model of the lava dome evolution can be used at other volcanoes during effusive eruptions, long episodes of lava dome building, the dome carapace formation and its potential failure, which may lead to pyroclastic flow hazards.

ACKNOWLEDGMENTS

We thank Juan Carlos Afonso, Tobias Keller and anonymous reviewer for their review and constructive comments. This is a contribution to the research project funded by the Deutsche Forschungsgemeinschaft (project DFG IS203/14–1). OM is supported by the PAUSE program (grant #C7H-PUB23A59). We are grateful to Vyacheslav Zobin for discussion on the dome growth at Volcán de Colima during 2007–2009.

DATA AVAILABILITY

The data supporting the conclusions of this paper and input model files for Ansys Fluent will be made available by the authors without undue reservation.

AUTHOR CONTRIBUTION

AIZ and NZ (a PhD student) contributed to the conceptualization of the paper. NZ processed the data, developed a numerical model and performed all model experiments. AIZ supervised the study and assisted NZ in numerical modelling and data processing. IT contributed to the development of numerical codes and modelling. AIZ, FS, NZ and OM contributed to interpretation of numerical results. AIZ and NZ performed writing–original draft preparation and figures. All co-authors performed writing–review and editing.

Competing Interests

The authors declare no competing interests.

SUPPORTING INFORMATION

Supplementary data are available at *GJI* online.

Figure S1. Temperature distribution in the models of lava dome growth in experiments 1.1(a) and 1.2(b).

Figure S2. The heat conduction term (a) and the viscous dissipation term (b) in experiment 1.2.

Please note: Oxford University Press is not responsible for the content or functionality of any supporting materials supplied by the authors. Any queries (other than missing material) should be directed to the corresponding author for the paper.

REFERENCES

Anderson, S.W. & Fink, J.H., 1990. The development and distribution of surface textures at the Mount St. Helens dome, in *Lava Flows and Domes; Emplacement Mechanisms and Hazard Implications,*pp. 25–46, ed. Fink, J.H., Springer.

Bretón-Gonzalez, M., Campos, A., Leon, Z., Plascencia, I. & Ramírez, J.J., 2013. The 2007-2012 lava dome growth in the crater of Volcán de Colima, México, derived from video monitoring system, in *Complex Monitoring of Volcanic Activity,* pp. 153–169, ed. Zobin, V.M., Nova Science Publishers Inc.

Calder, E.S., Lavallée, Y., Kendrick, J.E. & Bernstein, M., 2015. Lava dome eruptions, in *Encyclopedia of Volcanoes,* 2nd edn, pp. 343–362, eds Sigurdsson, H., Houghton, B., Rymer, H., Stix, J. & McNutt, S., Academic Press.

Cashman, K.V., 2020. Crystal size distribution (CSD) analysis of volcanic samples: advances and challenges, *Front. Earth Sci.,* **8,** 291.

Cimarelli, C., Costa, A., Mueller, S.P. & Mader, H.M.(2011). Rheology of magmas with bimodal crystal size and shape distributions: insights from analog experiments, *Geochem. Geophys. Geosys.,* **12,** 1–14.

Cordonnier, B., Lev, E. & Garel, F., 2015. Benchmarking lava-flow models, in *Detecting, Modelling and Responding to Effusive Eruptions,* Special Publications, **426,** pp. 425–445, eds Harris, A. J. L., De Groeve, T., Garel, F. & Carn, S. A., Geological Society.

Costa, A., 2005. Viscosity of high crystal content melts: dependence on solid fraction, *Geophys. Res. Lett.,* **32,** 1–5. 10.1029/2005GL024303..

Costa, A., Caricchi, L. & Bagdassarov, N., 2009. A model for the rheology of particle-bearing suspensions and partially molten tocks, *Geochem. Geophys. Geosys.,* **10**(3), doi:10.1029/2008GC002138.

Costa, A., Melnik, O. & Sparks, R.S.J, 2007a. Controls of conduit geometry and wall rock elasticity on lava dome eruptions, *Earth planet. Sci. Lett.,* **260,** 137–151.

Costa, A., Melnik, O. & Vedeneeva, E., 2007b. Thermal effects during magma ascent in conduits, *J. geophys. Res.,* **112**(B12), doi:10.1029/2007JB004985.

Costa, A., Wadge, G. & Melnik, O., 2012. Cyclic extrusion of a lava dome based on a stick-slip mechanism. *Earth planet. Sci. Lett.,* **337-338,** 39–46.

Courant, R., Friedrichs, K. & Lewy, H., 1928. Über die partiellen differenzengleichungen der mathematischen physik, *Math. Annal.,* **100**(1), 32–74.

Fink, J.H. & Griffiths, R.W., 1998. Morphology, eruption rates, and rheology of lava domes: insights from laboratory models, *J. geophys. Res.,* **103,** 527–545.

Frontoni, A., Costa, A., Vona, A. & Romano, C., 2022. A comprehensive database of crystal-bearing magmas for the calibration of a rheological model, *Sci. Data,* **9,** doi:10.1038/s41597-022-01363-w.

Griffiths, R.W., 2000. The dynamics of lava flows, *Ann. Rev. Fluid Mech.,* **32,** 477–518.

Hale, A.J., 2008. Lava dome growth and evolution with an independently deformable talus, *Geophys. J. Int.,* **174,** 391–417.

Hale, A.J. & Wadge, G., 2003. Numerical modeling of the growth dynamics of a simple silicic lava dome, *Geophys. Res. Lett.,* **30**(19), doi:10.1029/2003GL018182.

Hale, A.J., Wadge, G. & Mühlhaus, H.B., 2007. The influence of viscous and latent heating on crystal-rich magma flow in a conduit, *Geophys. J. Int.,* **171,** 1406–1429.

Harnett, C.E., Thomas, M.E., Purvance, M.D. & Neuberg, J., 2018. Using a discrete element approach to model lava dome emplacement and collapse, *J. Volc. Geotherm. Res.,* **359,** 68–77.

Harris, A.J., Rose, W.I. & Flynn, L.P., 2003. Temporal trends in lava dome extrusion at Santiaguito 1922–2000, *Bull. Volc.,* **65,** 77–89.

Hirt, C.W. & Nichols, B.D., 1981. Volume of fluid (VOF) method for the dynamics of free boundaries, *J. Comput. Phys.,* **39**(1), 201–225.

Husain, T., Elsworth, D., Voight, B., Mattioli, G. & Jansma, P., 2018. Influence of conduit flow mechanics on magma rheology and the growth style of lava domes, *Geophys. J. Int.,* **213,** 1768–1784.

Husain, T., Elsworth, D., Voight, B., Mattioli, G. & Jansma, P., 2019. Morphologic variation of an evolving dome controlled by the extrusion of finite yield strength magma, *J. Volc. Geotherm. Res.,* **370,** 51–64.

Husain, T., Elsworth, D., Voight, B., Mattioli, G.S. & Jansma, P., 2014. Influence of extrusion rate and magma rheology on the growth of lava domes: insights from particle-dynamics modelling, *J. Volc. Geotherm. Res.,* **285,** 110–117. 10.1016/j.jvolgeores.2014.08.013.

Hutchison, W., Varley, N., Pyle, D.M., Mather, T.A. & Stevenson, J.A., 2013. Airborne thermal remote sensing of the Volcán de Colima (Mexico) lava dome from 2007 to 2010, in *Remote Sensing of Volcanoes and Volcanic Processes: Integrating Observation and Modelling,* Vol. **380,** pp. 203–228, eds Pyle, D.M., Mather, T.A. & Biggs, J., Geological Society, London, Special Publications.

Ismail-Zadeh, A. & Tackley, P., 2010. *Computational Methods for Geodynamics*. Cambridge Univ. Press.

Iverson, R.M., 1990. Lava domes modeled as brittle shells that enclose pressurized magma, with application to Mount St. Helens, in *Lava Flows and Domes; Emplacement Mechanisms and Hazard Implications,* pp. 47–69, ed. Fink, J.H., Springer.

Kirkpatrick, R., 1976. Towards a kinetic model for the crystallization of magma bodies, *J. geophys. Res.,* **81,** 2565–2571. 10.1029/JB081i014p02565.

La Spina, G., Burton, M., Vitturi, M.D.M. & Arzilli, F., 2016. Role of syn-eruptive plagioclase disequilibrium crystallization in basaltic magma ascent dynamics, *Nat. Comm.,* **7**(1), 1–10.

Lavallée, Y. *et al.*, 2012. Magmatic architecture of dome building eruptions at Volcán de Colima, Mexico, *Bull. Volc.,* **74**(1), 249–260.

Lavallée, Y., Hess, K.U., Cordonnier, B. & Dingwell, D.B., 2007. A non-Newtonian rheological law for highly-crystalline dome lavas, *Geology,* **35,** 843–846. 10.1130/g23594a.1.

Lavallée, Y., Meredith, P., Dingwell, D.B., Hess, K.U., Wassermann, J., Cordonnier, B., Gerik, A. & Kruhl, J.H., 2008. Seismogenic lavas and explosive eruption forecasting, *Nature,* **453,** 507–510.

Lejeune, A. & Richet, P., 1995. Rheology of crystal-bearing silicate melts: an experimental study at high viscosity, *J. geophys. Res.,* **100,** 4215–4229.

Melnik, O. & Sparks, R.S.J., 1999. Nonlinear dynamics of lava dome extrusion, *Nature,* **402,** 37–41.

Mériaux, C.A., May, D.A. & Jaupart, C., 2022. The impact of vent geometry on the growth of lava domes, *Geophys. J. Int.,* **229**(3), 1680–1694.

Moore, G. & Carmichael, I.S.E., 1998. The hydrous phase equilibria (to 3 kbar) of an andesite and basaltic andesite from western Mexico: constraints on water content and conditions of phenocryst growth, *Contrib. Mineral. Petrol.,* **130,** 304–319. 10.1007/s004100050367.

Morse, S.A., 2011. The fractional latent heat of crystallizing magmas, *Amer. Mineral.,* **96,** 682–689. 10.2138/am.2011.3613.

Nakada, S. *et al.*, 2019. Growth process of the lava dome/flow complex at Sinabung Volcano during 2013–2016, *J. Volc. Geotherm. Res.,* **382,** 120–136. 10.1016/j.jvolgeores.2017.06.012.

Nakada, S., Shimizu, H. & Ohta, K., 1999. Overview of the 1990–1995 eruption at Unzen Volcano, *J. Volc. Geotherm. Res.,* **89,** 1–22. 10.1016/S0377-0273(98)00118-8.

Neri, A., 1998. A local heat transfer analysis of lava cooling in the atmosphere: application to thermal diffusion-dominated lava flows, *J. Volc. Geotherm. Res.,* **81,** 215–243. 10.1016/S0377-0273(98)00010-9.

Patankar, S.V. & Spalding, D.B., 1972. A calculation procedure for heat and mass transfer in three-dimensional parabolic flows, *Int. J. Heat Mass Transfer,* **15,** 1787–1806. 10.1016/0017-9310(72)90054-3.

Ramsey, M.S., Chevrel, M.O., Coppola, D. & Harris, A.J.L., 2019. The influence of emissivity on the thermo-rheological modeling of the channelized lava flows at Tolbachik volcano, *Ann. Geophys.,* **61,** doi:10.4401/ag-8077.

Reubi, O. & Blundy, J., 2008. Assimilation of Plutonic roots, formation of high-K exotic melt inclusions and genesis of andesitic magmas at Volcán De Colima, Mexico, *J. Petrol.,* **49**(12), 2221–2243.

Riker, J.M., Blundy, J.D., Rust, A.C., Botcharnikov, R.E. & Humphreys, M.C.S., 2015. Experimental phase equilibria of a Mount St. Helens rhyodacite: a framework for interpreting crystallization paths in degassing silicic magmas, *Contrib. Mineral. Petrol.,* **170**(6), doi:10.1007/s00410-015-1160-5.

Sheldrake, T.E., Sparks, R.S.J., Cashman, K.V., Wadge, G. & Aspinall, W.P., 2016. Similarities and differences in the historical records of lava dome-building volcanoes: implications for understanding magmatic processes and eruption forecasting, *Earth Sci. Rev.,* **160,** 240–263.

Starodubtseva, Y., Starodubtsev, I., Ismail-Zadeh, A., Tsepelev, I., Melnik, O. & Korotkii, A., 2021. A method for magma viscosity assessment by lava dome morphology, *J. Volc. Seismol.,* **15**(3), 159–168.

Tsepelev, I., Ismail-Zadeh, A. & Melnik, O., 2020. Lava dome morphology inferred from numerical modelling, *Geophys. J. Int.,* **223**(3), 1597–1609.

Tsepelev, I., Ismail-Zadeh, A., Starodubtseva, Y., Korotkii, A. & Melnik, O., 2019. Crust development inferred from numerical models of lava flow and its surface thermal measurements, *Ann. Geophys.,* **61**(2), doi:10.4401/ag-7745.

Tsepelev, I.A., Ismail-Zadeh, A.T. & Melnik, O.E., 2021. Lava dome evolution at Volcán de Colima, México during 2013: Insights from numerical modeling, *J. Volc. Seismol.,* **15** (6), 491–501.

Voight, B. & Elsworth, D., 2000. Instability and collapse of hazardous gas-pressurized lava domes, *Geophys. Res. Lett.,* **27**(1), 1–4.

Wadge, G., Robertson, R.E.A. & Voight, B.Eds. 2014. *The Eruption of Soufrière Hills Volcano, Montserrat, From 2000 to 2010,* Geol. Soc. London Mem., 39.

Walter, T.R. *et al.*, 2019. Imaging the 2013 explosive crater excavation and new dome formation at Volcan de Colima with TerraSAR-X, time-lapse cameras and modelling, *J. Volc. Geotherm. Res.,* **369,** 224–237.

Watts, R.B., Herd, R.A., Sparks, R.S.J. & Young, S.R., 2002. Growth patterns and emplacement of the andesitic lava dome at *Soufrière* Hills Volcano, Montserrat, in *The Eruption of Soufrière Hills Volcano, Montserrat, from 1995 to 1999,* Vol. **21,** pp. 115–152, eds Druitt, T.H. & Kokelaar, B.P., Geol. Soc. London Mem.

Zeinalova, N., Ismail-Zadeh, A., Melnik, O., Tsepelev, I. & Zobin, V., 2021. Lava dome morphology and viscosity inferred from data-driven numerical modeling of dome growth at Volcán de Colima, Mexico during 2007-2009, *Front. Earth Sci.,* **9,** doi:10.3389/feart.2021.735914.

Zobin, V.M. *et al.*, 2015. Dynamics of the January 2013–June 2014 explosive-effusive episode in the eruption of Volcán de Colima, México: insights from seismic and video monitoring, *Bull. Volc.,* **77**(31), doi:10.1007/s00445-015-0917-z.

Zobin, V.M. & Tellez, A., 2019. Precursors to intra-eruptive reposes during the 1998–2019 lava dome-building eruption at Volcán de Colima, México, *Bull. Volc.,* **81**(45), doi:10.1007/s00445-019-1307-8.

Zobin, V.M., Tellez, A., Aguilar, J.E. & Cruz, K.G., 2017. Seismic signals of rockfalls as indicators of the origin of lava fragments emplaced during the 2010 endogenous and exogenous growth in the crater of Volcán de Colima, México, *Bull. Volc.,* **79**(47), doi:10.1007/s00445-017-1130-z.